Application of a simplified model for assessing particle removal in dissolved air flotation (DAF) systems

Experimental verification at laboratory and full-scale level

Piaggio, Antonella L.; Smith, Geo; de Kreuk, Merle K.; Lindeboom, Ralph E.F.

DOI
10.1016/j.seppur.2024.126801

Publication date
2024

Document Version
Final published version

Published in
Separation and Purification Technology

Citation (APA)
Piaggio, A. L., Smith, G., de Kreuk, M. K., & Lindeboom, R. E. F. (2024). Application of a simplified model for assessing particle removal in dissolved air flotation (DAF) systems: Experimental verification at laboratory and full-scale level. *Separation and Purification Technology*, *340*, Article 126801. https://doi.org/10.1016/j.seppur.2024.126801

Separation and Purification Technology 340 (2024) 126801

Contents lists available at ScienceDirect

Separation and Purification Technology

journal homepage: www.elsevier.com/locate/seppur

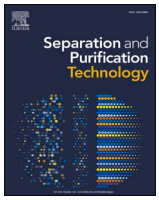

Application of a simplified model for assessing particle removal in dissolved air flotation (DAF) systems: Experimental verification at laboratory and full-scale level

Antonella L. Piaggio [a,*], Geo Smith [b], Merle K. de Kreuk [a], Ralph E.F. Lindeboom [a]

[a] Delft University of Technology, Faculty of Civil Engineering and Geosciences, Section Sanitary Engineering, Department of Water Management, Stevinweg 1, 2628 CN Delft, the Netherlands
[b] Nijhuis Saur Industries, Innovatieweg 4, 7007 CD Doetinchem, the Netherlands

ARTICLE INFO

Editor: T. Kuo-Lun

Keywords:
Dissolved air flotation (DAF)
Simplified model
Suspended solids
Particle image velocimetry (PIV)

ABSTRACT

Particle-bubble collisions in dissolved air flotation (DAF) systems play a crucial role in the removal of total suspended solids (TSS). DAF particle-bubble collision models incorporate factors such as particle diameters, charge and density, bubble diameters, and collision factors. The challenge lies in accounting for the wide range of particle and bubble sizes and obtaining complex model inputs. To address this, a simplified model for TSS removal in DAF units was established using low-cost laboratory measurements, including particle size distribution and density. Additionally, microbubble diameter profiles were derived from bubble velocities using particle image velocimetry software (PIV). Six independent variables, encompassing influent particle characteristics (such as particle size distribution and density) and DAF running characteristics (temperature, contact zone detention time, inflow and recycle flows), were employed in the simplified model. The model's accuracy was evaluated using a laboratory-scale DAF system with two different influents: Delft canal water and anaerobic sludge. The predicted TSS removal from the simplified model aligned well with the laboratory-scale DAF results, yielding removal efficiencies of 68 ± 1 % and 77 ± 3 % for Delft canal water and anaerobic sludge, respectively. Furthermore, when the simplified model was applied to two full-scale DAF systems, it successfully identified an underperforming system (DAF2) with a TSS removal efficiency of 91 %, contrasting with the theoretical removal model-predicted efficiency of 98 %. This study highlights the utility of combining bubble size distribution measured by PIVlab and particle size distribution obtained using FIJI-ImageJ as an economical and efficient approach to acquiring the necessary inputs for predicting TSS removal in DAF systems.

1. Introduction

Since the early 1960 s, an extensive application of dissolved air flotation (DAF) systems has been found for the separation of liquid and particles in drinking and wastewater. The first DAF systems were used in the 1920 s and aimed at recovering ores and valuable materials from water suspensions for exploitation in industries [1]. Before the 1970 s the Scandinavian countries were using DAF units for drinking water treatment, while some African countries were testing them for wastewater reclamation by algae removal on maturation ponds [2]. DAF units can get similar solids removal efficiencies as in settler tanks, but they do it in a shorter retention time and higher hydraulic loading rate. Suspended solids removal efficiency is between 60 and 99 %, while retention time can be from 3 to 60 min and, hydraulic loading rate between 2.5 and 12.5 $m^3.m^{-2}.h^{-1}$ [3–5]. Furthermore, the influent suspended solids rate might vary from 5.0 to 25.0 $kg.m^{-2}.h^{-1}$ [6]. The ability to deal with such a diversity of flows and solids content makes DAF systems suitable for treating particularly challenging streams, especially those with high variation in their flows and characteristics [7]. A summary of DAF units design parameters is shown in Table 1.

DAF removal efficiency of suspended solids is directly linked with the forming of bubble-particle aggregates [8]. The bubble-particle aggregate density plays a key role in its flotation or settling, and it depends on the bubble and particle characteristics. When the agglomerate density is lower than the water one, it will rise to the surface [6]. Most bubbles formed in DAF have diameters below 100 μm and rise as rigid spheres following Stokes law under laminar flow conditions [4]. If

* Corresponding author.
E-mail addresses: a.l.piaggio@tudelft.nl, antopiaggio@gmail.com (A.L. Piaggio), geo.smith@nijhuisindustries.com (G. Smith), M.K.deKreuk@tudelft.nl (M.K. de Kreuk), R.E.F.Lindeboom@tudelft.nl (R.E.F. Lindeboom).

https://doi.org/10.1016/j.seppur.2024.126801
Received 30 August 2023; Received in revised form 7 February 2024; Accepted 13 February 2024
Available online 17 February 2024

Nomenclature

Acronyms

A/S	Air to solids ratio
CFD	Computational fluid dynamics
DAF	Dissolved Air Flotation
HRT	Hydraulic retention time
PIV	Particle image velocimetry
PSD	Particle size distribution
SOLR	Solids' organic loading rate
TS	Total solids
TSS	Total suspended solids
VSS	Volatile suspended solids
WWTP	Wastewater treatment plant

Table 1
Typical DAF unit design parameters.

Parameters	Units	Ranges	Reference
Hydraulic Retention Time (HRT)	s	180–3600 1200–3600	Wang, et al. [8] Shammas, et al. [3]
Solids Organic Loading rate (SOLR)	$gTSS.m^{-2}.h^{-1}$	5,000–25,000	Metcalf, et al. [9]
Air to solids ratio (A/S)	$gAir.gTSS^{-1}.d^{-1}$	0.002–0.05	Wang, et al. [8]
Recycle flow	%	5–50 6–12	Wang, et al. [8] Edzwald [10]
Pressure	10^5Pa	2–6 4–6	Wang, et al. [6] Edzwald [10]
Coagulant concentration	$mg.L^{-1}$	500–2000	Haydar and Aziz [11]
Coagulation time	s	600–1800	Wang, et al. [8]

particles and the agglomerates are considered spheres, then Stokes law can be used to calculate the rising or settling velocity v_r [6,12], when one or more particles collide with one bubble, as shown in the equations below.

$$V_{pb} = \frac{\pi\left(n \times {d_p}^3 + {d_b}^3\right)}{6} \tag{1}$$

where V_{pb} corresponds to the agglomerate volume (m^3), n is the number of particles attached to the bubble, d_p and d_b are the particle and bubble diameters respectively (m).

$$d_{pb} = \left(\frac{6{V_{pb}}^3}{\pi}\right)^{\frac{1}{3}} \tag{2}$$

$$\rho_{pb} = \frac{\left(n\rho_p V_p + \rho_b V_b\right)}{V_{pb}} \tag{3}$$

where d_{pb} is the agglomerate diameters (m), ρ_p and ρ_b are the particle and bubble densities ($kg.m^{-3}$), and V_p and V_b are the particles and bubble volumes as solid spheres (m^3).

$$v_r = \frac{\left(\rho_w - \rho_{pb}\right) g {d_{pb}}^2}{18\mu} \tag{4}$$

Equation (4) shows the agglomerate velocity as v_r, where g is the gravitational constant (9.8 $m.s^{-2}$), ρ_w and μ are water density ($kg.m^{-3}$) and viscosity ($kg.m^{-1}.s^{-1}$) respectively.

Aside from density, the formation of the particle-bubble agglomerate also depends on the air bubbles' characteristics, like concentration and size. Bubble formation and concentration depend on the pressure set for DAF pressurised water. When air pressure is increased above atmospheric conditions in the saturation vessel, a higher concentration of dissolved air, mainly composed of nitrogen and oxygen is present in the liquid. Gas concentration in the liquid phase follows Henry's law, and depends on the selected pressure, temperature, and the gas Henry's constant [13] (equations (5) and (6). Table 2 shows Henry's constant for relevant gases.

$$H(T) = H^{\theta} e^{\left(\frac{-\Delta_{sol}H}{R}\left(\frac{1}{T}-\frac{1}{T^{\theta}}\right)\right)} \tag{5}$$

$$H(T) = \frac{c_a}{p} \tag{6}$$

where $H(T)$ corresponds to Henry's constant at temperature T (in Kelvin), T^{θ} refers to the temperature of 298.15 K, $\Delta_{sol}H$ corresponds to the dissolution enthalpy, R is the gas constant, c_a is the dissolved gas concentration, and p the partial pressure of the gas.

Once the air-pressurized liquid is released under atmospheric conditions, microbubbles are formed. These vary in diameter from 10 to 150 μm and are at least five times smaller than when fine bubble diffusers are used [4,15]. The total amount of bubbles formed once the pressurised water is released under atmospheric conditions depends on the bubble diameter. When air is used as a pressurizing gas, average microbubble diameters decrease with an increase in pressure, from 70 to 30 μm at 2 and 5×10^5 Pa respectively [16]. Nevertheless, when water is pressurized using CO_2, average microbubble diameters increase when pressure rises, from 100 to 200 μm at 2 and 3×10^5 Pa respectively [17]. For a given dissolved gas concentration, the total amount of released microbubbles will increase if the bubble diameter decreases [15].

Besides bubble characteristics, other factors also have an important effect on DAF performance. Particles' nature and size, solids loading rate, air-to-solids ratio (A/S), hydraulic retention time, and use of polymers and coagulants are among the most important factors to be considered [8]. Van Nieuwenhuijzen [18], established that most wastewater-suspended solids have a negatively charged surface. Likewise, air bubbles exhibit an extended range of pH-dependent negative zeta potential and surface charge [19]. To enhance collision between particles and bubbles, coagulants are used to neutralize particle surface charge. After adequate coagulation is achieved, flocculants are added to create bigger agglomerates. Thus, coagulation and flocculation are key to promoting particle-bubble agglomeration, and therefore, particle removal by flotation [20]. The highest suspended solids removal efficiency in a DAF system can be expected when particles and bubbles are similar in diameter size, and both have a surface zeta potential near zero. Han, et al. [21] state that a positive particle zeta potential (of 15 mV) shows a lower removal efficiency in the collision diagram, when compared to the one at 0 mV, due to the change from charge neutralization to sweep coagulation. Moreover, Han and Dockko [22] affirmed that when particle zeta potential is slightly over zero, high removal of particles can be expected. However, this might lead to an increase of 50 % of the coagulant dosage needed to reach neutral zeta potential [22,23]. The collision efficiency of bubble and particle (α_{bp}) is calculated using trajectory analysis. Particles below 10 μm are governed by Brownian diffusion and therefore, their trajectory can be impossible to predict in detail. Particles between 10 and 100 μm are mainly governed by interception [4]. This range is similar to the one of bubble sizes in the

Table 2
Henry's law constants for water as a solvent for relevant gases. Adapted from Sander [14].

	Henry's constant	$\Delta_{sol}H/R$
	$(mol.m^{-3}.Pa^{-1})$	(K)
Nitrogen	6.40E−06	1600
Oxygen	1.20E−05	1500
Carbon Dioxide	3.30E−04	2400
Methane	1.40E−05	1600

DAF system. Thus, the optimum particle removal in DAF units happens when particles and bubbles have similar sizes.

The majority of laboratory-scale DAF units testing particle removal can be considered bench-scale, and involve jar tests [7]. Whilst jar tests are optimal for the assessment of adequate coagulation and flocculation concentrations depending on the treated wastewater, they cannot replicate the bubble-particle collision. Thus, pilot-scale DAF units are recommended for further testing. Reported DAF units need large influent flows (between 5 and 100 $m^3.h^{-1}$), making it impossible to perform laboratory experiments with real wastewater [7]. Some authors have used laboratory-scale DAF units to empirically assess flow conditions, bubble formation, and bubble size [15,16,22,24,25]. Piaggio, et al. [26] used a down-scaled DAF unit to evaluate its performance under different influent conditions and system-independent variables, concluding the suitability of DAF units as a pretreatment step for solids removal of the Barapullah drain, New Delhi, India.

Most recent literature on DAF is linked to the utilization of computational fluid dynamics (CFD) based on the Navier-Stokes equations, to enhance understanding of the separation and behaviour in the contact zone [27]. However, the assessment of multiphase interactions between liquid (water), solids (particles) and gas (air bubbles) remains challenging [28]. Particle-bubble collision in the DAF contact zone has been modelled by Tambo and Fukushi [29], Edzwald [4], and Han [30]. The equations include particle diameters, charge, density, and bubble diameters. More recently, Koh and his co-workers developed a computational fluid dynamic–continuum particle model focused on simulating flotation systems [31–33]. While this model has a lower computational time when compared to other used models, it can still be considered complex, and it might introduce errors next to the system borders due to the wall-effect on the bubble and particle velocities [34]. The complexity of applying these models lies in the fact that both particles and bubbles are present in a wide variety of sizes [35].

Recent studies on DAF have also focused on the use of particle image velocimetry (PIV) as a tool to map the liquid velocity profile [36] and bubble velocity profiles [37]. The application of PIV has been mostly performed using high-speed cameras, to study bubble and particle dynamics [38]. However, PIV has not been used to assess the bubble diameter profile, and the possible interactions between liquid, bubbles, and particles.

To the author's knowledge, no scientific studies have been conducted on a simplified version of the model developed by Edzwald and co-workers, where low-cost laboratory measurements, such as particle size distribution and density, can be applied to achieve an initial approximation of suspended solids removal using a DAF unit. Furthermore, the authors have not found further investigation on the coupling of these bubble-particle collision models with laboratory-scale DAF units. This coupling might lead to a better understanding and assessment of the removal potential of DAF systems for different influents. Furthermore, the development of a simplified correlation model coupled with low-cost analytical measurements ensures the utilisation and testing of DAF units under economical and challenging environments, and under a diverse set of influents, which could represent the real-world conditions of changing waste- and drain-water.

2. Methods

2.1. Simplified particle removal model

Several heterogeneous flocculation-type models consider particle-trajectory equations regarding particle-bubble collision derived by Sutherland [39]. The filtration model developed by Edzwald and co-workers [4] was applied to calculate the expected suspended solids removal efficiency in the contact zone, using average bubble sizes and particle size distribution. This model, also known as the white-water bubble blanket model, considers the single-factor collision approach, where one bubble collides with a particle or floc. The model was first used for air filtration [40], and later to describe froth flotation [41]. It can be used when particle diameters are smaller than the average microbubble diameter [10].

The single-factor collector efficiency equations are derived from Brownian diffusion and particle transport mechanisms. When microbubbles have diameters below 120 μm, the velocities can be calculated using Stokes. The model starts with the second-order rate kinetics to describe the rate at which particles change due to their impact with bubbles. From there, equations (7) to (10) describe the total collision efficiency (η_T) and its components contributing to efficiency: Brownian diffusion (η_{BD}), interception (η_I), settling (η_S) and equation (11) shows the total removal efficiency (E_{CZ}) from the DAF contact zone. Collision due to inertia (η_{IN}) can be neglected when compared to the other collision factors when bubble and floc diameters are below 100 μm [7].

$$\eta_T = \eta_{BD} + \eta_I + \eta_S \tag{7}$$

$$\eta_{BD} = 6.18\left[\frac{k_b T}{g(\rho_w - \rho_b)}\right]^{2/3}\left[\frac{1}{d_p}\right]^{2/3}\left[\frac{1}{d_b}\right]^{2} \tag{8}$$

$$\eta_I = (\frac{d_p}{d_b}+1)^2 - \frac{3}{2}\left(\frac{d_p}{d_b}+1\right) + \frac{1}{2}(\frac{d_p}{d_b}+1)^{-1} \tag{9}$$

$$\eta_S = \left[\frac{(\rho_p - \rho_w)}{(\rho_w - \rho_b)}\right]\left[\frac{d_p}{d_b}\right]^{2} \tag{10}$$

where k_b is Boltzmann's constant (1.4×10^{-23} J.K^{-1}), T is the absolute temperature in Kelvin, g is the gravitational constant (9.8 m.s^{-2}), ρ_p, ρ_b, and ρ_w are the particle-floc, air bubble and water density (kg.m^{-3}), respectively, d_p and d_b are the particle and bubble diameter (m), respectively.

$$E_{cz} = \left[1 - exp\left(-\frac{3/2(\alpha_{pb}\eta_T v_b \varnothing_b t_{cz})}{d_b}\right)\right] \tag{11}$$

where α_{bp} is the collision efficiency factor for bubbles and particles, v_b is the air bubble velocity (m.s^{-1}), $\varnothing_b$ is the volume fraction of air in water, and t_{cz} is the DAF contact zone retention time (s).

Collision efficiency factors for bubble and particle α_{bp} were taken from Han [21,30], were based on bubble average size and assumed particle zeta potential close to zero (due to the addition of coagulants and flocculants). The methods used to calculate average bubble size and particle size distribution are explained below (Bubble size and, Particle size). Values of bubble velocity (v_b) were calculated based on the Stokes equation for rigid spheres (equation (4)). The volume fraction of air in water ($\varnothing_b$) depends on the dissolved air concentration and therefore, on the applied pressure, temperature conditions, and the recycle flow (equation (12)). A working pressure of 5×10^5 Pa was selected for the simplified model. Gas density and concentration were calculated based on the input temperature, Henry's constants for nitrogen and oxygen dissolution, air composition of 21 % oxygen and 79 % nitrogen, and assuming a 90 % efficiency of air dissolution [8].

$$\varnothing_b = \left(\varnothing_{bQr}\frac{Q_r}{Q_r + Q_{in}}\right) \tag{12}$$

where $\varnothing_b$ is the volume fraction of air in water ($L_{air}.L_{water}^{-1}$), $\varnothing_{bQr}$ is the volume fraction of air in water in the recycle flow ($L_{air}.L_{water}^{-1}$), calculated based on Henry's constant and applied pressure, and Q_r and Q_{in} are the recycle and influent flows, respectively.

For particles smaller than the average bubble size, the particle-bubble collision was calculated discretized per intervals of particle diameters of 10 μm, assuming a homogenous particle density, and then multiplied by particle frequency following the measured particle size distribution (PSD). The total collision efficiency per interval η_{Ti}, where i represents the particle interval, was calculated based on equation (11), and the total suspended particle removal was the sum of each interval

removal. To obtain the removal of particles with diameters equal to or bigger than the average bubble size diameter, the frequency of these particles (as a ratio of the total amount of particles) was multiplied by either the lowest possible removal efficiency, 50 %, or the highest expected removal efficiency, 90 % [42]. Thus, the model applied in this research predicts a removal range. A representation of the simplified model can be found in Appendix A**,** and the whole model can be found in Appendix E**.** The final inputs to run the model, as in independent (measured) and dependent parameters, are enumerated in Table 3.

For the experiments conducted in the laboratory-scale column DAF system, the selected DAF characteristics were a running temperature of 303 K (30 °C), contact zone detention time of 1200 s, an inflow flow of 0.017 ± 0.001 $m^3.h^{-1}$, and a recycle ratio of 1. These independent variables were selected based on the influent conditions to tests, and typical ranges of DAF parameters.

The independent parameters characterizing the particles and used for the simplified model were selected based on the need to perform low-cost and simple laboratory measurements. Particle size distribution can be directly measured using laser diffraction analysis, like Microtrac Bluewave (Malvern Instruments Ltd., UK), or assessed directly with a digital microscope and FIJI-ImageJ software, as described below (**Section 2.5**). This latter requires inexpensive instruments easily available in a laboratory.

Two dependent parameters were chosen for the model, the collision efficiency factor, and the average bubble diameter. While the latter is calculated based on PIV analysis of bubble velocities (described in **Section 2.3**), values of bubble diameters are not directly measured but derived from the velocities. The collision efficiency factor is dependent on the average bubble size and the assumption of adequate coagulation and flocculation.

2.2. Laboratory-scale DAF set-up

A laboratory-scale column DAF reactor was designed to measure bubble sizes and particle removal, as shown in Fig. 1. The system is similar to the one created by Piaggio, et al. [26], and located at TU-Delft (Delft, Netherlands). The DAF column system dimensions were a height of 1.00 m and a diameter of 0.2 m, and it was made from polymethyl methacrylate. The column dimensions were chosen to minimize the wall effect on particle movement inside the DAF column, as mentioned by Edzwald [4]. Influent injection and effluent retrieval were located at 0.20 m from the bottom of the system, diametrically opposed. A stainless steel 10 L Thielman reactor was used to store tap water that was pressurized to 5.0 × 10^5 Pa. The pressurized water flow (white water flow) was released at atmospheric conditions and mixed with the tested influent through a T connection, and afterwards injected into the system via a polyurethane tubing of 4 mm internal diameter (PUN-6x1-SI, FESTO, Esslingen, Germany). The white-water flow rate was controlled through a one-way needle valve (Festo 193969, Esslingen, Germany),

The influent and white-water flows were set to be similar, using an influent pump (Watson Marlow 520). On the influent injection point, at 0.20 m from the bottom of the system, a connection tube with identical dimensions as the influent tube above described, was placed vertically, and positioned centrally to promote an upstream flow and enhance particle removal. The concentrate flow was removed from a height of 0.65 m above the column bottom at the fourth collection point, from both sides of the column.

Before the beginning of each trial, both for bubble size measurement and suspended particle removal assessment, the DAF column was filled with tap water to a height of 0.65 m.

Table 3
Particle-bubble collision simplified model inputs and units.

Inputs			Units
Independent variables	Particle characteristics	Particle size frequency in intervals of 10 μm*	%
		Particle density	g. cm^{-3}
	DAF characteristics	Running temperature	K
		Contact zone detention time (τcz)	s
		Inflow flow (Qin)	$m^3.h^{-1}$
		Recycle ratio (R)**	%
Dependent variables	Particle-bubble interaction	Collision efficiency factor (αbp)	–
	Bubble characteristics	Average bubble diameter	μm

*As a percentage of the total amount of particles
** The recycle ratio (R) is equivalent to the white-water flow, and calculated as a percentage of the Q_{in}

2.3. Bubble size calculation using particle image velocimetry (PIV)

Bubble size experiments were conducted in the laboratory-scale column DAF. The experiments were conveyed using tap water, and a pressure of 5.0 × 10^5 Pa. LED lights were mounted at the top and back of the DAF column in a square formation. Then the DAF column with the LED lights was covered with a black bag to create opaque surroundings and enhance image quality [43]. A slit was created in the black bag at the front side of the DAF, big enough to locate a mobile phone camera without enabling light infiltration from outside. Unlike in previous work, no high-speed camera, but a mobile phone camera (MI6, Xiaomi, Beijing, China) was used to record the bubble rise slow-motion videos. The camera was 12 megapixels, had a 1,334 × 750-pixel resolution (high resolution – 4 K), and was able to tape at slow motion taking 30 frames per second.

For the bubble experimental trials, the influent (containing tap water) flow pump and white-water flow were opened at the same time, for a total duration of 145 s. After this period, both inflows to the laboratory-scale DAF column were stopped. Videos were recorded from the moment the influent and white water were on, and for a further 40 s after they were off, representing a total video time of 185 s. Afterwards, the videos were cut into 10-second sub-videos (equivalent to 300 frames). Two sub-videos per run, corresponding to times between 135 and 145 and 165 to 175 s were analysed to assess bubble velocities. These videos were called "*Tap water 2*" (135–145 s), and "*Tap water 3*" (165–175 s). The selection of the first video frame was done bearing in mind that both inflows (influent and white-water) were on during the record. For the second video frame, bubble movement was not affected by influent flows.

Particle image velocimetry (PIV) was applied to analyse the recorded videos and compute the bubble velocities. Particularly, the PIVlab MATLAB package was used to process the videos [43]. In PIV, a velocity map is obtained based on a sequence of images, by determining the shift of particles from consecutive frames, at a defined time interval [44]. Vertical and horizontal velocity components every 0.5 mm were obtained in a grid of approximately 30 mm × 10 mm, giving a total of around 1200 velocity points in each grid. Calibration of the velocity vectors was performed based on the time elapsed between two consecutive video frames (30 fps), and a ruler that was installed inside the DAF column system. The horizontal and vertical velocity outputs were then used to calculate the bubble diameters correlated to the obtained velocities using Stokes (equation (4)). Finally, average bubble sizes per grid (of two consecutive frames) were determined based on the total bubble sizes calculated per each velocity point.

2.4. Particle removal in the laboratory-scale DAF

Two different influents were assessed for suspended solids removal in the laboratory-scale column DAF. Firstly, drain water from a canal located in the vicinity of TU-Delft (Van der Burghweg, Delft, The Netherlands) was collected. This water was chosen due to its solid's

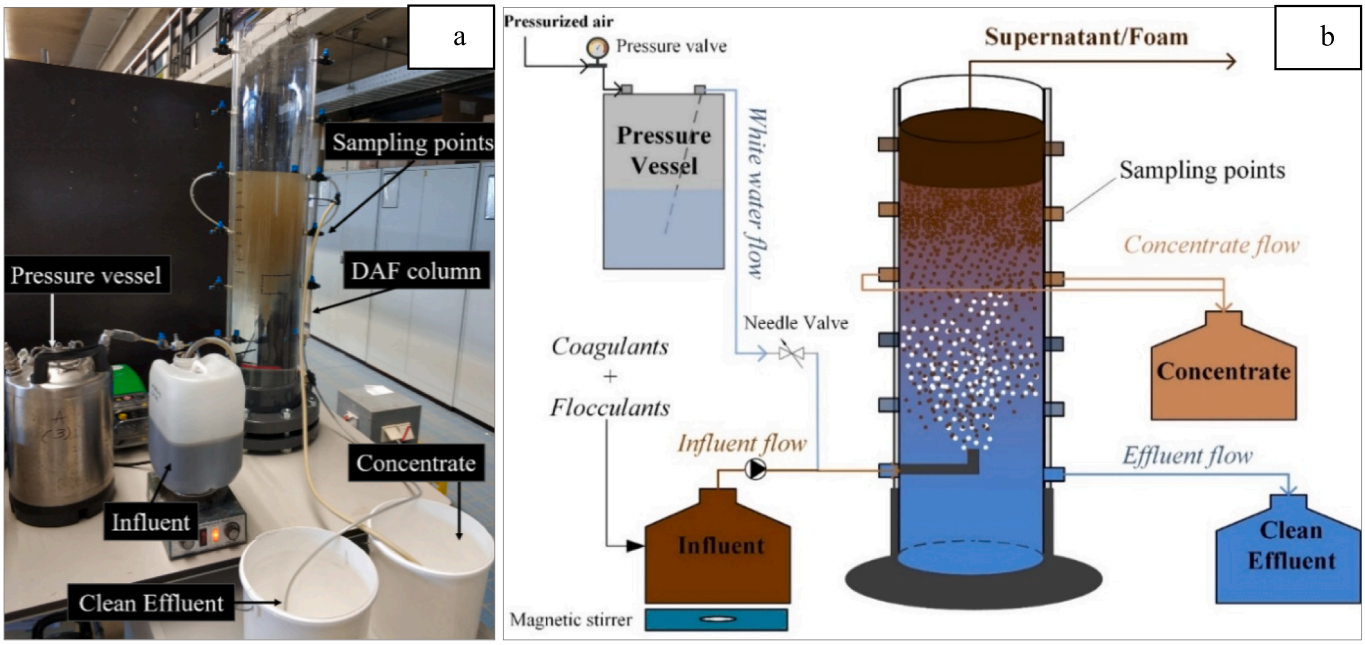

Fig. 1. Laboratory-scale column DAF system located in the Water Lab facilities (TU-Delft, The Netherlands). a. A picture taken from the laboratory, b. a schematic image of the DAF system.[26].

characteristics since it is expected that canal water has a high content of small and inorganic solids. Delft canal water pH was 7.8 ± 0.1, total and suspended solids concentrations (TS and TSS) were 840 ± 48 mgTS.L^{-1}, and 32 ± 7 mgTSS.L^{-1}. The second tested influent was anaerobically digested sludge from a domestic Wastewater Treatment Plant (WWTP), located at Den Hoorn, Netherlands (RWZI–Harnaschpolder, Netherlands). To avoid clogging the laboratory-scale DAF, the sludge was sieved with a 0,71 mm filter. After sieving, the sludge pH was 6.9 ± 0.1, TS concentration was 37.3 ± 0.1 gTS.L^{-1}, and TSS concentration was 36.8 ± 1.5 gTSS.L^{-1}. The anaerobic sludge was diluted with Delft canal water until a TSS concentration of 0.5 gTSS.L^{-1}.

2.4.1. Laboratory-scale column DAF runs

Suspended solids removal in the laboratory-scale DAF column was evaluated for Delft canal water and the anaerobically digested sludge. The total running time of each experiment was around 20 min (1200 s). Influent and white-water flows were fed into the system for the first 810 s. For the first 300 s, the effluent valve was kept closed, and the DAF column height increased up to a total volume of 25 L. Then the effluent valve was opened and kept open for another 300 s. The concentrate extraction points, located in the upper part of the lab column, were opened at 900 s, and the concentrate flow was discharged by gravity until the water height in the laboratory-scale column reached 0.65 m (extraction point). This process took on average 1200 s. A schematic of the laboratory-scale DAF runs can be seen in Fig. 2.

2.5. Particle size

Particle characteristics and morphology were evaluated following the method described by Piaggio, et al. [26] with a digital microscope (VHX-5000 Series, KEYENCE, Osaka, Japan) and FIJI-ImageJ processing software [45]. At least nine high-definition images taken from the tested influent, were stacked together and then further processed with FIJI-ImageJ software to analyse the particles' size distribution. For each measured particle, FIJI-ImageJ software was set to give the measurements of particle area, perimeter, and circularity, using a known distance in the stacked pictures (0.854 pixel.μm^{-1}). Particle circularity can be between zero to one, being one a perfect circle [46]. Particle diameters were then calculated assuming all particles as spheres based on the values of particle area given by FIJI-ImageJ. Particle frequency every 10 μm was calculated by dividing the number of observed particles in a diameter range, by the total number of counted particles in the stacked image.

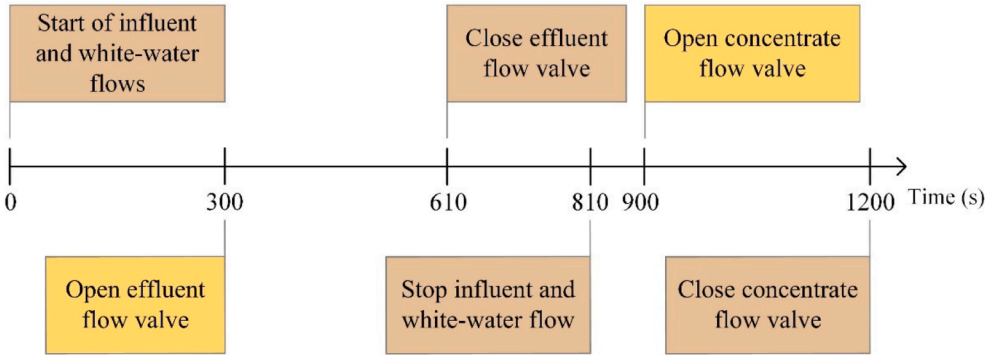

Fig. 2. Laboratory-scale DAF column experimental times.

2.6. Analytical methods

Total solids (TS) and total suspended solids (TSS) were measured following the Standard Method [47] and performed in triplicates. Measurements of pH at TU-Delft Lab facilities were conducted using and WTW multi720 pH meter. Finally, particle density was measured via a 100 mL pycnometer (Blaubrand, Wertheim, Germany), following Blake and Hartge [48].

3. Results and discussion

3.1. Microbubble sizes

The horizontal and vertical velocity vector components for each frame were extracted by implementing PIVlab, and absolute average bubble horizontal and vertical velocities were calculated for the videos *Tap water 2* and *Tap water 3*. For *Tap water 2* and *Tap water 3*, the average absolute bubble vertical velocities were $9.0 \times 10^{-3} \pm 1.3 \times 10^{-2}$ m.s^{-1}, and $2.7 \times 10^{-3} \pm 1.2 \times 10^{-3}$ m.s^{-1}, respectively. Average absolute bubble horizontal velocities were $6.5 \times 10^{-3} \pm 1.1 \times 10^{-2}$ m.s^{-1} and $5.3 \times 10^{-4} \pm 4.4 \times 10^{-2}$ m.s^{-1} for *Tap water 2* and *Tap water 3,* respectively. A higher absolute horizontal velocity and standard deviation were obtained for the *Tap water 2* video. This was also observed when absolute average velocities were calculated per frame and not only for the whole recording.

The difference between the bubble velocities of *Tap water 2* and *Tap water 3* can be due to the mixing conditions brought by the influent flow, which was running while recording the video *Tap water 2* and closed for *Tap water 3*. In the videos captured during the experiment, it was observed that bubbles from *Tap Water 3* follow a more linear trend when compared to *Tap Water 2*. The water flow recorded during *Tap Water 2* affected the free bubble movement, and therefore, cannot be used coupled with Stokes law to determine bubble sizes. The difference between the velocity vectors at 140 and 170 s (from *Tap water 2* and *Tap water 3* respectively) is shown in Fig. 3. The first one has higher bubble flow disturbance leading to a vast variation in velocity direction, while at 170 s, bubble velocity vectors are mostly vertically aligned. Furthermore, bubbles observed during the recording of *Tap water 2* were of a larger scale than the ones in the video *Tap water 3*. Baeyens, et al. [49] found that water depressurization can produce bubbles of around 1 mm in diameter which can disturb the laminar flow and floc formation and therefore, should be removed in the contact zone.

Using the vertical velocity vectors, bubble sizes were calculated. Bubble diameters per mesh point were calculated based on velocity data and the Stokes equation. The hypothesis to be able to apply Stokes are that the bubbles should be considered spherical spheres, with smooth surface, and flowing in a laminar flow. This latter means that the Reynolds number should be below 2000 [50]. Thus, after applying Stokes equation to calculate the bubble diameters, the values of Reynolds numbers linked to each velocity and bubble diameter were calculated and assessed, following the equation below.

$$R_e = \frac{\rho_L \times v \times d_b}{\mu} \tag{13}$$

where ρ_L is water density, v and d_b are the absolute vertical velocity and diameter of the bubble, and μ is the water dynamic viscosity (all values were considered at 15 °C).

Stokes' assumption of the movement of bubbles as solids spheres is only valid for Reynolds numbers in the order of 1. Furthermore, the application of Stokes leads to calculating the relative velocity between one bubble (or particle) and the liquid around it. Thus, the use of this equation is not fully correct for a dense quantity of bubbles. Bearing in mind that during the recording of *Tap water 3* there were a smaller number of bubbles in comparison to *Tap water 2*, and the tap water was off (minimizing the water movement), the video *Tap water 3* was selected for the assessment of bubble diameters, while the video *Tap water 2* was discarded. Moreover, the application of Stokes for bubble diameter and Reynolds number led to the identification of a maximum bubble diameter of 1.4 mm in the recorded video *Tap water 2* (subjected to a hydraulic loading rate of around 1 m^3.m^{-2}.h^{-1}), and a maximum Reynolds number of 1182.

The average velocity per frame for the *Tap water 3* followed a linear

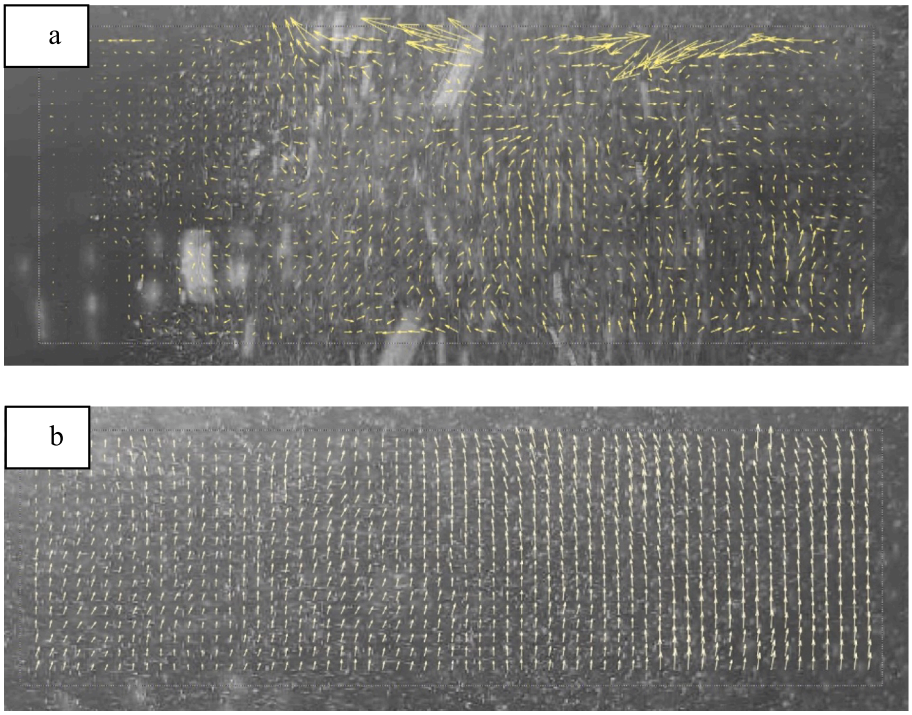

Fig. 3. Velocity vectors from PIVlab. a corresponds to the velocity vector extracted from Tap water 2 at 140 s. b shows the same conditions taken from Tap water 3 at 170 s. Both images are representative of what is observed in each tap water recording.

decrease over time (R^2 of 0.92) (Appendix B). Concomitantly to the decrease in bubble velocity, a decrease in the standard deviation of these velocities was also observed. Based on the vertical velocity values, average bubble diameters were calculated (Fig. 4). Average bubble sizes linearly decrease over time (R^2 of 0.92) from 83 to 69 μm. The obtained bubble velocity and diameter profiles are aligned with what is expected from the theory. When the pressurized influent was released into the laboratory-scale DAF column, a cluster of bubbles with various sizes were formed. The larger the bubble diameter the higher the vertical velocity, as shown in Stokes equation (equation (4). Therefore, the bigger bubbles are expected to float first, followed by the smaller bubbles. When observations are made at a fixed distance from the white-water inlet, the bubbles with higher velocity (and corresponding higher bubble diameters) will be observed first, in comparison to those with lower velocities. Furthermore, the smaller bubbles are expected to spend longer periods inside the column in comparison to bigger ones and therefore, lower bubble diameters should be expected at the end of the recording in comparison to the beginning of it.

From the whole *Tap water 3* recording, bubble sizes followed a positively skewed distribution (Fig. 5), where the average diameter was 74 ± 15 μm, and minimum and maximum values corresponded to 2 μm and 196 μm. The 95 % confidence interval showed that most bubbles have a size between 50 and 110 μm. These values are in the same range as what is stated in the literature, with sizes between 20 and 150 μm [15,16]. Moreover, the bubble size distribution followed a similar trend to the one estimated by Vlyssides, et al. [51] and measured by Rodrigues and Rubio [52]. The distribution was positively skewed, where higher velocities far from the peak are more frequent than lower ones.

While the bubble size profile obtained using PIV resembles the results found in previous models, the average bubble diameter of 74 μm at 5×10^5 Pa is bigger than expected (30 to 40 μm [15,52]). Several factors might affect bubble diameter. Firstly, the narrowing opening of a valve or nozzle, causing bubble formation due to cavitation, could cause bubble coalescence and therefore, bigger bubble diameters [15]. Moreover, during image analysis, overlapping of bubbles can be observed, and bigger bubbles can be present. As a result, the velocity profile obtained using PIV can be derived for larger bubble diameters [52]. Even though this is a constraint of using PIV, bubble interactions inside a DAF system will naturally occur and the coalescence of several bubbles will form bigger ones. When using the average bubble diameter on the simplified model, suspended solid removal could be overestimated. Smaller bubbles are beneficial for suspended solids removal since they provide higher surface areas available for collision [10].

3.2. Simplified model results and verification with values from the laboratory-scale DAF

Average values of bubble diameter from *Tap water* 3 were used in combination with the particle characteristics needed to run the experimental suspended solids removal model. PSD results for both Delft canal water and Harnaschpolder anaerobic digested sludge are shown in Fig. 6. More than half of the particles of Delft canal water had a diameter size below 10 μm, while this value was 35 % for the Harnaschpolder anaerobic sludge. Furthermore, 5 % of the anaerobic sludge particles had a size above 120 μm, while the maximum particle size for Delft canal water was 80 μm. Appendix C includes particle images of both influents used for PSD calculations. The measured average particle density was 1.08 ± 0.02 g.cm^{-3} for Delft canal water and 1.04 ± 0.03 g.cm^{-3} for the anaerobic sludge.

Results of the removal models applied to both influents showed that the suspended solids removal for Delft canal water should be 68 ± 1 %, while this value for Harnaschpolder anaerobic sludge should be 77 ± 3 %. For both influents, the most important collision factor between bubbles and particles was interception (η_I). This coefficient was one or two orders of magnitude above the Brownian diffusion (η_{BM}) and settling (η_S) coefficients. Edzwald [4] found that Brownian diffusion governs the collision possibility of particles and bubbles, for particles diameters below 1 μm, while interception governs the collision for particles above 1 μm. In the simplified model, particles with sizes below 10 μm were the hardest to remove. These particles had the lowest chance of collision with bubbles, due to their small surface area available and interception coefficient, with 52 and 43 % chance of collision for the anaerobic sludge and the Delft canal water, respectively.

The laboratory-scale column DAF was used to evaluate the removal efficiency of suspended solids and compare the results to the predictive model. For the Delft canal water, with a TSS concentration of around 30 mgTSS.L^{-1}, the removal varied between 66 and 96 %, while for the anaerobic sludge with a concentration of 500 mgTSS.L^{-1}, the removal was between 68 and 92 %, when five experimental runs were conducted per influent type [26]. The simplified model predicted removals of 68 ± 1 % and 77 ± 3 % for Delft canal water and the anaerobic sludge, respectively. These predicted values are aligned with the removals obtained in the laboratory-scale column. Furthermore, if the influents are subjected to good coagulation and flocculation, and the frequency of particles below 10 μm halved, the simplified model predicts an increase of suspended solids removal to 84 and 88 % for the Delft canal water and anaerobic sludge, respectively.

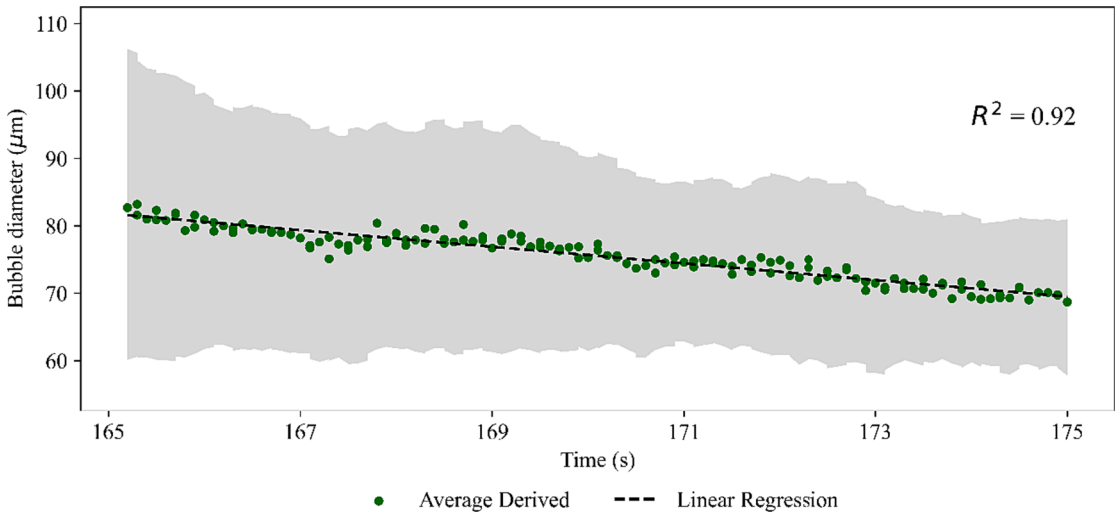

Fig. 4. Average bubble diameter and standard deviation (in grey shadows). The diameters were calculated using Stokes and the velocity magnitudes were obtained from PIVlab. The figure is based on the video Tap water 3, recorded between 165 and 175 s, where there was no inflow into the laboratory-scale DAF column.

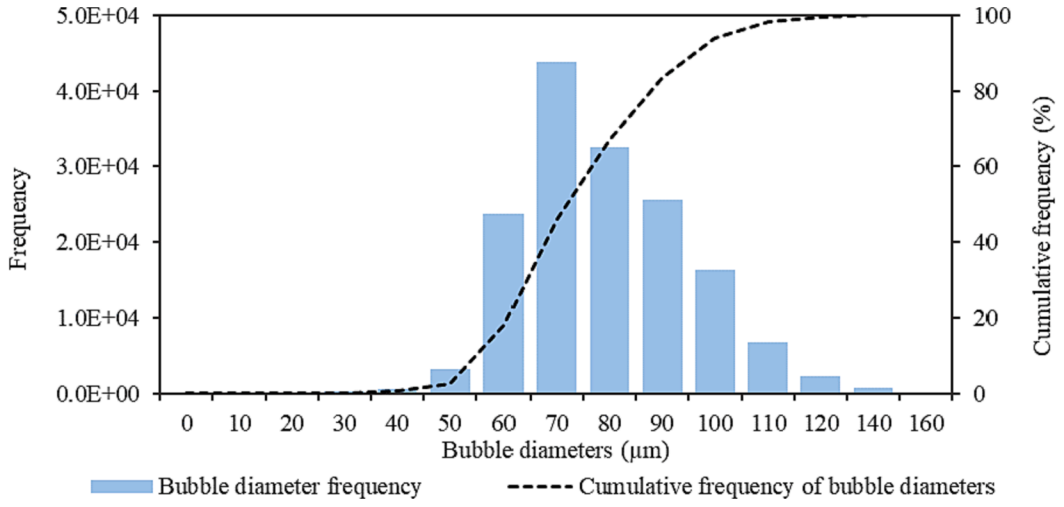

Fig. 5. Bubble size distribution based on diameters, for the recorded video entitled Tap water 3.

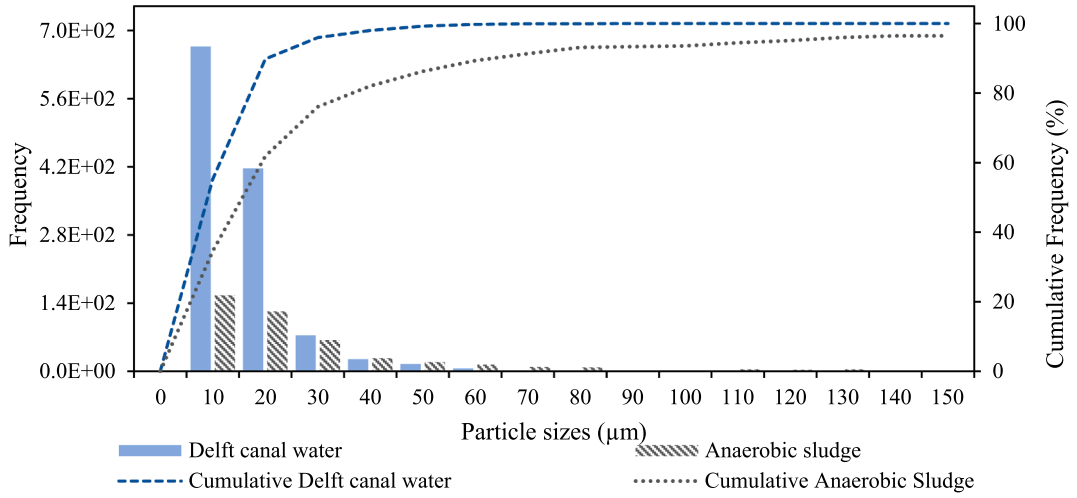

Fig. 6. Particle size distribution (PSD) for Delft canal water and Harnaschpolder anaerobic digested sludge. The values were obtained using microscope images and the FIJI-ImageJ software to analyse particle shapes and their corresponding diameter. The calculations of PSD were conducted based on the total amount of measured particles. The microscope images used to gather particle shape and size can be found in Appendix C.

While the simplified model gave a similar range of suspended solids removal to the one assessed in the laboratory-scale DAF column, the model has limitations. Firstly, the simplified model was run using only the average bubble diameter and not the full bubble size distribution. Depending on the bubble size distribution in the DAF unit, the simplified model can over or underestimate the suspended solids removal. A change in the average bubble size from 74 to 50 µm increases the predicted TSS removal efficiencies of Delft canal water and anaerobic sludge by 5 %, to 76 and 82 %, respectively. Likewise, an increase in average bubble size to 90 µm had a negative effect of reducing the predicted TSS removal by 3 % to the Delft canal water and anaerobic sludge, respectively. Thus, the effect of average bubble size in the predicted removal efficiencies varies depending on the influent particle characteristics and might lead to significant changes. The sensitivity and uncertainty linked to this dependent model variable should be further assessed to better describe the interactions between particles and bubbles.

Secondly, values of the collision efficiency factor (α_{bp}) were taken from Han [21]. Trajectory analysis is used to calculate the α_{bp} factor, which depends on particle size and density, zeta potential, bubble wall effect, and fluid turbulence [53]. Generally, the rate of particle-bubble attachment has been analysed based on three main factors, which are the probability of actual collision, the probability of attachment occurring once the collision happened, and the collision frequency based on linear interception [54]. For particles above 30 µm, the bubble surface effect on the particle drag force might decrease the collision efficiency [55]. The collision efficiency factor effect is mostly predominant in the removal of small particles. In the simplified model, an α_{bp} decrease of 20 % shows a reduction of 4 and 2 % in TSS removal of Delft canal water and anaerobic sludge, respectively. If α_{bp} further decreases to 60 % of its original value, then the TSS removal prediction in Delft canal water plunges by 8 %. Thus, the sensitivity of the collision efficiency factor in the simplified model should be further assessed to enhance model prediction.

The model considers that the influent particles and agglomerates have a zeta potential close to zero (adequate coagulation and flocculation), but the zeta potential was not measured during the experiments conducted in the laboratory-scale DAF. Regular techniques of measuring adequate coagulation and flocculation involve jar tests for different polymer concentrations [7]. The method to measure PSD developed in this study could be useful as a complementary assessment of adequate coagulation and flocculation. Typical equipment employed to measure PSD, when particle sizes are smaller than a millimetre, uses light scatter techniques [56]. The use of this technique requires setting a liquid flow

(water) with the particles to analyse, passing through a laser beam. Solids aggregates can be weak and get destroyed in the process [57]. Thus, the alternative method using microscope images and FIJI-ImageJ software can be considered to efficiently measure the particle aggregates.

Finally, the model considers that all particles have a homogenous density and surface. Drain- and wastewater particles are heterogeneous, they can be inert or organic, and be categorised as settleable or not. Around 30 % of the total suspended solids in domestic wastewater can be considered inert [58]. From the tested influents, Delft canal water was expected to have a higher inert matter content than the anaerobically digested sludge. This can be observed based on the average particle density of both influents, 1.08 and 1.04 $g.cm^{-3}$ for Delft canal water anaerobic sludge, respectively. Nevertheless, both influents have a combination of organic and inorganic particles. Thus, considering that all particles from the influent have the same particle density might lead to wrong predictions of particle removal.

3.3. Experimental prediction model and verification in full-scale DAF performance

Two full-scale DAF systems were used to compare the results of the simplified model and the suspended solids removal in the laboratory-scale DAF. The DAF systems were used as part of an industrial wastewater treatment plant. The treatment consisted of a DAF unit (DAF1) used for pre-treatment, followed by a biological nitrogen and phosphorus removal unit, with aerobic and anaerobic times. Finally, a second DAF system (DAF2) was used as a polishing step after the biological unit. The DAF systems were in the Netherlands and supplied by Nijhuis Saur Industries. Samples of influents (after coagulation and flocculation), and effluents from the DAF systems were collected to analyse. DAF units' influent characteristics and suspended solids removal are shown in Table 4. The PSD of each influent can be seen in Appendix D. Both units had influent flows around 10 $m^3.h^{-1}$, a recycle flow (R) ratio of 1, and were run under a white-water pressure of 5×10^5 Pa.

Results from the application of the simplified model with an average bubble size of 74 μm showed that both DAF units could reach a suspended solids removal efficiency of 98 ± 1 % and 96 ± 1 % for DAF1 and DAF2, respectively. While this was the case in practice for DAF2 (98 %), the DAF1 unit was running under a lower removal efficiency than the predicted one, namely 91 %. The suspended removal efficiencies obtained in the tested full-scale DAF systems are similar to what several researchers observed. Ansari, et al. [59] found a TSS removal of 98.5 % when a full-scale DAF system was used as a pre-treatment of wastepaper-recycling wastewater. Furthermore, Rattanapan, et al. [60] observed a suspended solids removal efficiency of almost 100 % when using a DAF unit with acidification and coagulation to treat biodiesel wastewater. Finally, Koivunen and Heinonen-Tanski [61] achieved a 95 % reduction of suspended solids when a pilot-scale DAF was used to treat primary effluent of municipal wastewater.

When taking the full-scale DAF samples for testing, the DAF1 was not working under optimal conditions. Influent pH after coagulation and flocculation was too low (around 3.5), and prone to affect the following treatment steps. This was reflected in the results of the simplified model, where under optimal coagulation and flocculation, the DAF1 unit is expected to achieve a suspended solids removal of around 98 %. Chemical pre-treatment, to neutralize particle charge and form bigger agglomerates, is essential for DAF efficiencies [62,63]. When inorganic coagulants and flocculants are used, like aluminium or iron salts, low pH promotes coagulation by accelerating the hydrolysis of coagulants to Al^{+3} and Fe^{+3} [64]. Zhao, et al. [65] concluded that to obtain adequate coagulation of oily wastewater the pH should be kept below 7. Furthermore, anionic polymer flocculants are highly affected by small changes in pH, and pH values below 4.5 are not recommendable [65]. Thus, the difference between the expected removal of the DAF1 and the actual obtained TSS removal could be due to the low influent pH.

Moreover, the influent of the DAF1 was at a temperature of 40 °C. A lower amount of bubbles can be expected to be released under these conditions in comparison to normal conditions [13]. Air dissolution in water at a pressure of 5×10^5 Pa decreases around 30 % when temperatures increase from 20 to 40 °C. Thus, fewer bubbles can be expected to form under higher temperatures, reducing the chances of collision between bubbles and particles. Furthermore, the air and water density, and the water viscosity are also affected by the increase in temperature, concomitantly influencing the bubbles velocities. For an average bubble size of 74 μm, temperature increase from 20 to 40 °C rises the bubble velocity by 50 %, from 0.30 to 0.45 $cm.s^{-1}$, respectively. The rise in bubble velocities reduces the time the bubbles are inside the DAF system, reducing the chances of collision with particles.

Finally, the simplified model for DAF suspended solids removal proved to be aligned with the results obtained in the full-scale DAF systems and gave information regarding the level of optimization of the systems. While the DAF2 was working under optimal suspended solids removal conditions, the model results indicated that DAF1 performance could be enhanced, resulting in the advice to improve the influent pH and temperature control. Results of the DAF2 simplified model and model can be found in Appendix E (excel file).

4. Conclusions

A simplified model for total suspended solids (TSS) removal on dissolved air flotation (DAF) units was developed using the single-factor collision approach. A set of six independent variables were used for the simplified model. These variables referred to influent particle characteristics: particle size distribution (PSD) and particle density, and DAF running characteristics: temperature, contact zone detention time, inflow and recycle flows. Two dependent variables, collision efficiency factor and average bubble diameter, were used as model inputs. The latter was derived from measurements of bubble velocities using particle image velocimetry. The model was verified using a laboratory-scale DAF system evaluated for two different influents (Delft canal water and anaerobic sludge), and on two full-scale DAF installations. The main conclusions of this paper are as follows:

- The developed simplified model was able to predict the TSS removal efficiencies of a laboratory-scale column DAF system when two different influents were used. Results from the model showed a TSS removal of 68 ± 1 %, and 77 ± 3 % for Delft canal water and the anaerobic sludge, respectively, while experimental removals were between 66 and 96 % for Delft canal water and 68 to 92 % for anaerobic sludge.

Table 4
Full-scale DAF systems influent characteristics and suspended solids removal efficiencies. DAF1 was located at the beginning of the wastewater treatment train, while DAF2 was located after the biological removal of nitrogen and phosphorus.

	Particle density	Influent pH	Influent TSS	Influent temperature	TSS removal	Predicted TSS removal
	$g.cm^{-3}$	–	$g.L^{-1}$	K	%	%
DAF1	1.06 ± 0.014	3.5	1.86 ± 0.06	313	91 ± 2	98 ± 1
DAF2	1.07 ± 0.002	7.5	10.71 ± 0.32	293	98 ± 1	96 ± 1

- When modelling two full-scale DAF units, results from the simplified model showed that one of the units was underperforming, with a measured TSS removal of 91 % and an expected one of 98 %. Thus, the model was able to identify potential improvements.
- The sizes of microbubbles produced when depressurizing water can be measured using easily available materials, like a mobile camera, and PIV software. Furthermore, the derived bubble size distribution using the method described in this research proved to be aligned with the theory.
- Particle removal was shown to be greatly affected by the particle size distribution. Thus, adequate coagulation and flocculation are key to improving particle removal by flotation.

The average bubble diameter, influent particle size distribution and density, were key inputs for the simplified model. The measurement of these parameters was performed using easily available computational tools and simple inexpensive experimental procedures. These methods could overcome the difficulties of performing laboratory or pilot-scale TSS removal tests for assessing the efficiency of DAF systems.

Author Contributions

The manuscript was written through the contributions of all authors. All authors have approved the final version of the manuscript and contributed to the manuscript as follows: [*] [+] [-] research conception and design; [*] [#]data collection; [*] [+] [-]analysis and interpretation of results; [*] [#] [+] [-]draft manuscript preparation.

CRediT authorship contribution statement

Antonella L. Piaggio: Writing – review & editing, Writing – original draft, Visualization, Methodology, Investigation, Formal analysis, Data curation. **Geo Smith:** Writing – review & editing, Supervision, Conceptualization. **Merle K. de Kreuk:** Writing – review & editing, Writing – original draft, Supervision, Resources, Project administration, Investigation, Funding acquisition, Conceptualization. **Ralph E.F. Lindeboom:** Writing – review & editing, Visualization, Supervision, Project administration, Funding acquisition, Data curation, Conceptualization.

Declaration of competing interest

The authors declare the following financial interests/personal relationships which may be considered as potential competing interests: Merle K. de Kreuk reports financial support was provided by Dutch Research Council.

Data availability

Data will be made available on request.

Acknowledgements

This research was funded by NWO in the Netherlands (Project number 15424-2) and the Department of Biotechnology (DBT) in India (BT/IN/Indo-Dutch/19/TRS/2016), as part of the LOTUS-HR program (https://lotushr.org). Our gratitude goes to Nijhuis for all the inputs on DAF and the supplied information regarding the dull-scale DAF systems. The authors are grateful for the help of the lab technicians at the TU Delft Water Lab.

Appendix A. Supplementary material

Supplementary data to this article can be found online at https://doi.org/10.1016/j.seppur.2024.126801.

References

[1] H. Kiuri, Development of dissolved air flotation technology from the first generation to the newest (third) one (DAF in turbulent flow conditions), Water Sci. Technol. 43 (8) (2001) 1–7, https://doi.org/10.2166/wst.2001.0450.
[2] J. Haarhoff, Dissolved air flotation: progress and prospects for drinking water treatment, J. Water Supply: Res. Technol.—AQUA 57 (8) (2008) 555–567, https://doi.org/10.2166/aqua.2008.046b.
[3] N.K. Shammas, L.K. Wang, H.H. Hahn, Fundamentals of wastewater flotation, in: Flotation Technology, vol. 12. Humana Press, Totowa, NJ, 2010, pp. 121-164.
[4] J. Edzwald, Principles and applications of dissolved air flotation, Water Sci. Technol. 31 (3–4) (1995) 1–23, https://doi.org/10.1016/0273-1223(95)00200-7.
[5] H.J. Kiuru, Unit operations for the removal of solids and their combinations in water treatment, in: Chemical water and wastewater Treatment, Springer, 1990, pp. 169–186.
[6] M.M. Benjamin, D.F. Lawler, Water quality engineering: Physical/chemical treatment processes, John Wiley & Sons, New York, 2013.
[7] Edzwald and Haarhoff, Dissolved air flotation for water clarification, first ed. McGraw Hill Professional, 2011.
[8] Wang, Fahey, Wu, Dissolved air flotation, in: Physicochemical treatment processes, vol. 3: Humana Press, 2005, pp. 431-500.
[9] Metcalf, et al., Wastewater engineering: treatment and resource recovery, McGraw Hill Education, 2014.
[10] Edzwald, Dissolved air flotation and me, Water Res. 44 (7) (2010) 2077–2106, https://doi.org/10.1016/j.watres.2009.12.040.
[11] S. Haydar, J.A. Aziz, Coagulation–flocculation studies of tannery wastewater using combination of alum with cationic and anionic polymers, J. Hazard. Mater. 168 (2–3) (2009) 1035–1040, https://doi.org/10.1016/j.jhazmat.2009.02.140.
[12] P. Jenicek, J. Koubova, J. Bindzar, J. Zabranska, Advantages of anaerobic digestion of sludge in microaerobic conditions, Water Sci. Technol. 62 (2) (2010) 427–434, https://doi.org/10.2166/wst.2010.305.
[13] J.H. van 't Hoff, Etudes de dynamique chimique, Muller, 1884.
[14] R. Sander, Compilation of Henry's law constants (version 4.0) for water as solvent, Atmos. Chem. Phys. 15(8) (2015).
[15] S.E. De Rijk, J.G. den Blanken, Bubble size in flotation thickening, Water Res. 28 (2) (1994) 465–473, https://doi.org/10.1016/0043-1354(94)90284-4.
[16] Han, Park, Lee, Shim, Effect of pressure on bubble size in dissolved air flotation, Water Science and Technology: Water Supply, 2(5-6) (2002) 41–46, doi: https://doi.org/10.2166/ws.2002.0148.
[17] D.-H. Kwak, M.-S. Kim, Feasibility of carbon dioxide bubbles as a collector in flotation process for water treatment, J. Water Supply Res Technol. 62 (1) (2013) 52–65, https://doi.org/10.2166/aqua.2013.156.
[18] A.F. Van Nieuwenhuijzen, Scenario studies into advanced particle removal in the physical-chemical pre-treatment of wastewater, 2002. Available.
[19] M. Han, S. Dockko, Zeta potential measurement of bubbles in DAF process and its effect on the removal efficiency, KSCE J. Civ. Eng. 2 (4) (1998) 461–466, https://doi.org/10.1007/BF02830128.
[20] J. Bratby, Coagulation and flocculation, first ed., Crydon, England, 1980.
[21] M. Han, W. Kim, S. Dockko, Collision efficiency factor of bubble and particle (abp) in DAF: theory and experimental verification, Water Sci. Technol. 43 (8) (2001) 139–144, https://doi.org/10.2166/wst.2001.0484.
[22] Han, Dockko, Zeta potential measurement of bubbles in DAF process and its effect on the removal efficiency, KSCE J. Civ. Eng. 2(4) (1998) 461-466, doi: https://doi.org/10.1007/BF02830128.
[23] A. Van Nieuwenhuijzen, A. Mels, Characterisation of particulate matter in municipal wastewater, in: Chemical water and wastewater treatment VII. International Water Association (IWA), London, 2002, pp. 203-212.
[24] R.F. Mudde, O. Simonin, Two-and three-dimensional simulations of a bubble plume using a two-fluid model, Chem. Eng. Sci. 54 (21) (1999) 5061–5069, https://doi.org/10.1016/S0009-2509(99)00234-1.
[25] R.W. Samstag, et al., CFD for wastewater treatment: an overview, Water Sci. Technol. 74 (3) (2016) 549–563, https://doi.org/10.2166/wst.2016.249.
[26] A.L. Piaggio, L.A. Soares, M. Balakrishnan, T. Guleria, M.K. de Kreuk, R. E. Lindeboom, High suspended solids removal of Indian drain water with a down-scaled Dissolved Air Flotation (DAF) for water recovery. Assessing water-type dependence on process control variables, Environ. Challenges (2022) 100567, https://doi.org/10.1016/j.envc.2022.100567.
[27] D.F. del Yang, E. Pozo, U. Torfs, D.Y. Rehman, I. Nopens, "Numerical simulation on the effects of bubble size and internal structure on flow behavior in a DAF tank: A comparative study of CFD and CFD-PBM approach, Chem. Eng. J. Adv. 7 (2021) 100131, https://doi.org/10.1016/j.ceja.2021.100131.
[28] G. Wang, L. Ge, S. Mitra, G.M. Evans, J. Joshi, S. Chen, A review of CFD modelling studies on the flotation process, Miner. Eng. 127 (2018) 153–177, https://doi.org/10.1016/j.mineng.2018.08.019.
[29] N. Tambo, K. Fukushi, A kinetic study of dissolved air flotation, Presented at the World Congress of Chemical Engineering, Tokyo, 1986.
[30] Han, Modeling of DAF: the effect of particle and bubble characteristics, J. Water Supply: Res. Technol.-AQUA 51(1) (2002) 27–34, doi: https://doi.org/10.2166/aqua.2002.0003.
[31] P. Koh, M. Manickam, M. Schwarz, CDF simulation of bubble-particle collisions in mineral flotation cells, Miner. Eng. 13 (14–15) (2000) 1455–1463, https://doi.org/10.1016/S0892-6875(00)00130-8.
[32] P. Koh, M. Schwarz, Modelling attachment rates of multi-sized bubbles with particles in a flotation cell, Miner. Eng. 21 (12–14) (2008) 989–993, https://doi.org/10.1016/j.mineng.2008.02.021.

[33] G. Lane, P. Koh, CFD simulation of a Rushton turbine in a baffled tank, in: Proc. Int. Conf. CFD in Mineral and Metal Processing and Power Generation, CSIRO, Melbourne, 1997, pp. 377–385.
[34] R. Krishna, M.V. Urseanu, J. Van Baten, J. Ellenberger, Wall effects on the rise of single gas bubbles in liquids, Int. Commun. Heat Mass Transfer 26(6) (1999) 781-790, doi: https://doi.org/10.1016/S0735-1933(99)00066-4.
[35] R.T. Rodrigues, J. Rubio, DAF–dissolved air flotation: Potential applications in the mining and mineral processing industry, Int. J. Miner. Process. 82 (1) (2007) 1–13, https://doi.org/10.1016/j.minpro.2006.07.019.
[36] V.R. Fanaie, M. Khiadani, T. Ayres, Effects of internal geometry on hydrodynamics of dissolved air flotation (DAF) tank: an experimental study using particle image velocimetry (PIV), Colloids Surf. A Physicochem. Eng. Asp. 575 (2019) 382–390, https://doi.org/10.1016/j.colsurfa.2019.05.027.
[37] V.R. Fanaie, M. Khiadani, Effect of salinity on air dissolution, size distribution of microbubbles, and hydrodynamics of a dissolved air flotation (DAF) system, Colloids Surf. A Physicochem. Eng. Asp. 591 (2020) 124547, https://doi.org/10.1016/j.colsurfa.2020.124547.
[38] R. Lindeboom, G. Smith, D. Jeison, H. Temmink, J.B. van Lier, Application of high speed imaging as a novel tool to study particle dynamics in tubular membrane systems, J. Membr. Sci. 368 (1–2) (2011) 95–99, https://doi.org/10.1016/j.memsci.2010.11.029.
[39] K. Sutherland, Physical chemistry of flotation. XI. Kinetics of the flotation process, J. Phys. Chem. 52 (2) (1948) 394–425.
[40] S.K. Friedlander, D. Smoke, and Haze, 1977.
[41] L. Flint, W. Howarth, The collision efficiency of small particles with spherical air bubbles, Chem. Eng. Sci. 26 (8) (1971) 1155–1168, https://doi.org/10.1016/0009-2509(71)87002-1.
[42] K.-I. Fukushi, Y. Matsui, N. Tambo, Dissolved air flotation: experiments and kinetic analysis, J. Water Supply: Res. Technol.—AQUA 47 (2) (1998) 76–86, https://doi.org/10.2166/aqua.1998.13.
[43] W. Thielicke, E. Stamhuis, PIVlab–towards user-friendly, affordable and accurate digital particle image velocimetry in MATLAB, J. Open Res. Software 2(1), 2014, doi: https://doi.org/10.5334/jors.bl.
[44] A. Haidari, W. van der Meer, One Step Membrane Filtration: A fundamental study, Doctoral thesis Doctoral Dissertation, Delft University of Technology, Netherlands, 2017.
[45] J. Schindelin, et al., Fiji: an open-source platform for biological-image analysis, Nat. Methods 9 (7) (2012) 676–682, https://doi.org/10.1038/nmeth.2019.
[46] T. Ferreira, W. Rasband, ImageJ User Guide: IJ 1.46r, National Institute of Health. https://imagej.nih.gov/ij/docs/guide/ (accessed 17TH mARCH, 2022).
[47] American Public Health Association, APHA. 2005, Standard Methods for the Examination of Water and Wastewater. 21st ed. American Public Health Association, Washington DC, 1220p, 2013.
[48] G. Blake, K. Hartge, Particle density, Methods of soil analysis: Part 1 physical and mineralogical methods, vol. 5, pp. 377-382, 1986, doi: https://doi.org/10.2136/sssabookser5.1.2ed.c14.
[49] J. Baeyens, I. Mochtar, S. Liers, H. De Wit, Plugflow dissolved air flotation, Water Environ. Res 67 (7) (1995) 1027–1035, https://doi.org/10.2175/106143095X133266.
[50] S.A. Ahmed, D.P. Giddens, Velocity measurements in steady flow through axisymmetric stenoses at moderate Reynolds numbers, J. Biomech. 16 (7) (1983) 505–516, https://doi.org/10.1016/0021-9290(83)90065-9.
[51] A.G. Vlyssides, S.T. Mai, E.M.P. Barampouti, Bubble size distribution formed by depressurizing air-saturated water, Ind. Eng. Chem. Res. 43 (11) (2004) 2775–2780, https://doi.org/10.1021/ie0307176.
[52] R. Rodrigues, J. Rubio, New basis for measuring the size distribution of bubbles, Miner. Eng. 16 (8) (2003) 757–765, https://doi.org/10.1016/S0892-6875(03)00181-X.
[53] T.Y. Liu, M. Schwarz, CFD-based modelling of bubble-particle collision efficiency with mobile bubble surface in a turbulent environment, Int. J. Miner. Process. 90 (1–4) (2009) 45–55, https://doi.org/10.1016/j.minpro.2008.10.004.
[54] A. Nguyen, H.J. Schultze, Colloidal science of flotation (Surfactant science series). Marcel Dekker Inc, 2004, p. 850.
[55] T. Liu, M. Schwarz, CFD-based multiscale modelling of bubble–particle collision efficiency in a turbulent flotation cell, Chem. Eng. Sci. 64 (24) (2009) 5287–5301, https://doi.org/10.1016/j.ces.2009.09.014.
[56] H. Li, J. Li, J. Bodycomb, G.S. Patience, Experimental methods in chemical engineering: particle size distribution by laser diffraction—PSD, Can. J. Chem. Eng. 97 (7) (2019) 1974–1981, https://doi.org/10.1002/cjce.23480.
[57] A. Bieganowski, et al., An improved method for determination of aggregate stability using laser diffraction, Land Degrad. Dev. 29 (5) (2018) 1376–1384, https://doi.org/10.1111/jfs.12369.
[58] M. Henze, M.C. van Loosdrecht, G.A. Ekama, D. Brdjanovic, Biological wastewater treatment, IWA publishing, 2008.
[59] S. Ansari, J. Alavi, Z.M. Yaseen, Performance of full-scale coagulation-flocculation/DAF as a pre-treatment technology for biodegradability enhancement of high strength wastepaper-recycling wastewater, Environ. Sci. Pollut. Res. 25 (34) (2018) 33978–33991, https://doi.org/10.1007/s11356-018-3340-0.
[60] C. Rattanapan, A. Sawain, T. Suksaroj, C. Suksaroj, Enhanced efficiency of dissolved air flotation for biodiesel wastewater treatment by acidification and coagulation processes, Desalination 280 (1–3) (2011) 370–377, https://doi.org/10.1016/j.desal.2011.07.018.
[61] J. Koivunen, H. Heinonen-Tanski, Dissolved air flotation (DAF) for primary and tertiary treatment of municipal wastewaters, Environ. Technol. 29 (1) (2008) 101–109, https://doi.org/10.1080/09593330802009410.
[62] A. Al-Shamrani, A. James, H. Xiao, Destabilisation of oil–water emulsions and separation by dissolved air flotation, Water Res. 36 (6) (2002) 1503–1512, https://doi.org/10.1016/S0043-1354(01)00347-5.
[63] D. Leppinen, A kinetic model of dissolved air flotation including the effects of interparticle forces, J. Water Supply: Res. Technol.—AQUA 49 (5) (2000) 259–268, https://doi.org/10.2166/aqua.2000.0022.
[64] A. Zouboulis, P. Moussas, F. Vasilakou, Polyferric sulphate: Preparation, characterisation and application in coagulation experiments, J. Hazard. Mater. 155 (3) (2008) 459–468, https://doi.org/10.1016/j.jhazmat.2007.11.108.
[65] C. Zhao, et al., Application of coagulation/flocculation in oily wastewater treatment: A review, Sci. Total Environ. 765 (2021) 142795, https://doi.org/10.1016/j.scitotenv.2020.142795.